Emergence of a Fermionic Finite-Temperature Critical Point in a Kondo Lattice

Po-Hao Chou,[1] Liang-Jun Zhai,[1] Chung-Hou Chung,[2] Chung-Yu Mou,[1,3,4] and Ting-Kuo Lee[3]
[1]Department of Physics, National Tsing Hua University, Hsinchu 30013, Taiwan, Republic of China
[2]Electrophysics Department, National Chiao-Tung University, HsinChu 30010, Taiwan, Republic of China
[3]Institute of Physics, Academia Sinica, Nankang 115, Taiwan, Republic of China
[4]Physics Division, National Center for Theoretical Sciences, P.O.Box 2-131, Hsinchu 30013, Taiwan, Republic of China
(Received 7 January 2016; published 27 April 2016)

The underlying Dirac point is central to the profound physics manifested in a wide class of materials. However, it is often difficult to drive a system with Dirac points across the massless fermionic critical point. Here by exploiting screening of local moments under spin-orbit interactions in a Kondo lattice, we show that below the Kondo temperature, the Kondo lattice undergoes a topological transition from a strong topological insulator to a weak topological insulator at a finite temperature T_D. At T_D, massless Dirac points emerge and the Kondo lattice becomes a Dirac semimetal. Our analysis indicates that the emergent relativistic symmetry dictates nontrivial thermal responses over large parameter and temperature regimes. In particular, it yields critical scaling behaviors both in magnetic and transport responses near T_D.

DOI: 10.1103/PhysRevLett.116.177002

Since the discovery of graphene [1,2], enormous efforts have been inspired to search for materials with similar Dirac-like electronic structures. It was soon realized that a variety of materials, known as topological insulators, can exhibit low-dimensional Dirac Fermions at surfaces [3–5] due to the nontrivial topology in bulk electronic structures. More recently, 3D Dirac semimetallic phases were also found in Na_3Bi [6] and Cd_3As_2 [7,8]. In these materials, the underlying Dirac points are central to the associated novel properties [9] and the mass of the Dirac fermions is the energy gap that controls the transition between the topological trivial and the topological nontrivial phases [4,10,11]. Right at the point when the mass vanishes, the material is a Dirac semimetal which is at the fermionic quantum critical point (QCP) between the hole Fermi liquid and the electron Fermi liquid [12]. The quantum criticality extends effects of the Dirac point to a finite critical regime [12] and results in nontrivial scalings in Dirac semimetals. Despite the profound physics that can be manifested in Dirac semimetals, access to the critical point requires particular symmetries [13] and they are rare in real materials. Furthermore, the transition across the critical point requires tunability of electronic structures. Successful manipulations of electronic states across the critical point are often difficult [11] and are usually not performed in the same system. It is therefore desirable to search for feasible ways to access the fermionic critical point.

In this work, we explore topological phases at finite temperatures due to the many-body screening interaction of localized spins and conduction electrons in a Kondo lattice. We demonstrate that the hybridization of localized spins and conduction electrons leads to temperature-dependent electronic energy bands with the mass of the Dirac fermions being tunable. When spin-orbit interactions are included in hybridization, we find that the Kondo lattice is a strong topological insulator at low temperature [14] and undergoes a topological transition to a weak topological insulator at a higher temperature T_D. At T_D, Dirac points emerge and the system is a Dirac semimetal. Our results indicate that the finite temperature transition through a Dirac semimetallic phase results in nontrivial critical scaling behaviors both in transport and magnetic responses near T_D.

The model.—We start with the Anderson lattice Hamiltonian (ALH) on a cubic lattice, which is shown to characterize the topological Kondo insulating phase of SmB_6 [14],

$$H = \sum_{\mathbf{k}\sigma}(\xi_{\mathbf{k}} c^{\dagger}_{\mathbf{k}\sigma} c_{\mathbf{k}\sigma} + \xi^{d}_{\mathbf{k}} d^{\dagger}_{\mathbf{k}\sigma} d_{\mathbf{k}\sigma}) + \sum_{\mathbf{k}\sigma\sigma'}(V^{\sigma\sigma'}_{\mathbf{k}} c^{\dagger}_{\mathbf{k}\sigma} d_{\mathbf{k}\sigma'} + \text{H.c.}) + U\sum_{i} n^{d}_{i\uparrow} n^{d}_{i\downarrow}. \quad (1)$$

Here $c^{\dagger}$ and $d^{\dagger}$ create conduction and more localized electrons in the f orbit, respectively. $\xi_{\mathbf{k}}$ is equal to $\varepsilon_{\mathbf{k}} - \mu$ with $\varepsilon_{\mathbf{k}} = -2t\sum_{i=x,y,z}\cos k_i - 4t'\sum_{i\neq j}\cos k_i \cos k_j$ and μ being the chemical potential. $\xi^{d}_{\mathbf{k}} = \varepsilon_d - \eta\varepsilon_{\mathbf{k}} - \mu$ characterizes the narrow band formed by d electrons with η being the bandwidth and ε^d being the relative shift of band center. $\mathbf{V}_{\mathbf{k}}$ is the hybridization between c and d electrons, given by $v_0 I + 2\lambda_{\text{so}}\sum_{i=x,y,z}\sigma_i \sin k_i$ with I and σ_i being the unit and the Pauli matrices, respectively. Here v_0 vanishes due to the odd parity of the f orbits [14] so that the spin-orbit interaction λ_{so} dominates. Finally, U describes the Hubbard repulsion between d electrons.

Kondo screening.—We first analyze the screening interaction between c and d electrons. In the presence of λ_{so}, effective spin interactions are modified. By applying the Schrieffer-Wolff transformation [15] on the ALH in the

continuum limit with $\varepsilon_d - \mu = -U/2$ [16], we obtain the generalized Kondo lattice Hamiltonian [22] with three types of spin interactions represented by (i) the Heisenberg interaction $J_1 \vec{s}_{\mathbf{k}\mathbf{k}'} \cdot \vec{s}_d$, (ii) the Dzyaloshinskii-Moriya interaction $J_2[-i(\vec{k} - \vec{k}') \cdot (\vec{s}_{kk'} \times \vec{s}_d)]$, and (iii) the tensor type interaction $J_3[(\vec{s}_{kk'} \cdot \vec{k})(\vec{k}' \cdot \vec{s}_d) + (\vec{s}_{kk'} \cdot \vec{k}')(\vec{k} \cdot \vec{s}_d)]$, where $\vec{s}_{\mathbf{k}\mathbf{k}'} = \psi^\dagger_{\mathbf{k}} \vec{\sigma} \psi_{\mathbf{k}'}$ and $\vec{s}_d = \phi^\dagger_d (\vec{\sigma}/2) \phi_d$ with $\psi_{\mathbf{k}} = (c_{\mathbf{k}\uparrow}, c_{\mathbf{k}\downarrow})$ and $\phi^\dagger_d = (d^\dagger_\uparrow, d^\dagger_\downarrow)$. The strengths of spin interactions are given by $J_1 = J v_0^2$, $J_2 = J v_0 \lambda_{\mathrm{so}}$, $J_3 = 4 J \lambda_{\mathrm{so}}^2$ with $J = 1/(U + \varepsilon_d - \mu) - 1/(\varepsilon_d - \mu)$. The screening of a single localized spin is analyzed by a renormalization group (RG) analysis [23]. By defining dimensionless parameters $g_i = 2\rho J_i$ with ρ being the density of states at the Fermi energy, we obtain coupled flow equations [16]: $\dot{g}_1 = -(g_1^2 + g_2^2)$, $\dot{g}_2 = -g_2(g_1 + g_3)$, $\dot{g}_3 = -(g_3^2 + g_2^2)$. Here the solution is $(g_1 - g_3)/(g_2) = \mathrm{const}$. The initial coupling constants at the band cutoff D_0 satisfy $g_1(D_0) g_3(D_0) = g_2^2(D_0)$. We find that all the g_i's flow to infinity at the Kondo temperature [16]

$$T_K = D_0 e^{[-1/2\rho(J_1 + J_3)]}. \tag{2}$$

T_K is clearly enhanced in comparison to the Kondo temperature without λ_{so}, $T_K^0 = D_0 e^{(-1/2\rho J_1)}$. This enhancement persists even when many localized spins are included [16].

λ_{so} also changes the screening scenario below T_K. This is exhibited by performing the decomposition: $C_{\mathbf{k}\sigma} = (1/k) \sum_{lm} \mathrm{Y}_l^m(\hat{k}) C_{lk\sigma}^m$ with Y_l^m being spherical harmonics. Because the hybridization only mixes the orbital angular momentum $l = 1$ with spins, the $d_{\uparrow/\downarrow}$ electron only couples c electrons with $j_z = \pm 1/2$ through a particular linearly combined $C_{1k\sigma}^{m\dagger}$ defined by $a^\dagger_{k,j_z=\pm 1/2} = v_0 C^{0\dagger}_{0k,\pm 1/2} \pm v_1 (C^{0\dagger}_{1k,\pm\frac{1}{2}} - \sqrt{2} C^{\pm 1\dagger}_{1k,\mp\frac{1}{2}})$ with $v_1 = (2/\sqrt{3}) \lambda_{\mathrm{so}} k_F$ [16]. The resulting spin interaction is $J_1 \vec{s}_{\mathbf{k}\mathbf{k}'} \cdot \vec{s}_d$ with $\vec{s}_{\mathbf{k}\mathbf{k}'} = \sum_{\alpha,\beta} a^\dagger_{k,\alpha} \vec{\sigma}_{\alpha\beta} a_{k,\beta}$. Hence it is the total angular momenta of c electrons that interact with the d electron. Below T_K, c, and d electrons are coupled with the total angular momentum being screened. However, since d electrons only couple to $a^\dagger_{k,j_z=\pm 1/2}$, other linear combinations of $C_{1k\sigma}^{m\dagger}$ are left free [16]. This hints that more structures may exist in the phase space below T_K.

Topological phase diagram.—To access electronic structures below T_K in the large U limit, we apply the slave-boson method by expressing $d^\dagger_{i\sigma} = f^\dagger_{i\sigma} b_i$, where f_i and b_i are spinon and holon operators satisfying the constraint, $\sum_\sigma f^\dagger_{i\sigma} f_{i\sigma} + b_i^\dagger b_i = 1$. The constraint is removed by a Lagrangian field λ_i so that the Hamiltonian has to include the extra term $\sum_i \lambda_i (\sum_\sigma f^\dagger_{i\sigma} f_{i\sigma} + b_i^\dagger b_i - 1)$. In the mean field approximation, holons condense with $\langle b_i \rangle = \langle b_i^\dagger \rangle \equiv r$ and λ_i is replaced its mean-field value λ. The Hamiltonian becomes $H_M = \sum_{\mathbf{k}\sigma} (c_{\mathbf{k}\sigma}, f_{\mathbf{k}\sigma})^\dagger H_{\mathbf{k}} (c_{\mathbf{k}\sigma}, f_{\mathbf{k}\sigma}) + N\lambda(r^2 - 1)$ with

$$H_{\mathbf{k}} = \begin{pmatrix} \xi_{\mathbf{k}} I & r \mathbf{V}_{\mathbf{k}} \\ r \mathbf{V}_{\mathbf{k}} & \tilde{\xi}^d_{\mathbf{k}} I \end{pmatrix}. \tag{3}$$

Here N is the number of sites and $\tilde{\xi}^d_{\mathbf{k}} = (\varepsilon_d + \lambda) - \eta r^2 \varepsilon_{\mathbf{k}} - \mu$. It is convenient to rewrite $\xi_{\mathbf{k}} = m_{\mathbf{k}} - \mu_{\mathbf{k}}$ and $\tilde{\xi}^d_{\mathbf{k}} = -m_{\mathbf{k}} - \mu_{\mathbf{k}}$ with $m_{\mathbf{k}} = [(1 + \eta r^2)\varepsilon_{\mathbf{k}} - \varepsilon_d - \lambda/2]$ and $\mu_{\mathbf{k}} = \mu - [(1 - \eta r^2)\varepsilon_{\mathbf{k}} + \varepsilon_d + \lambda/2]$. By minimizing the free energy, r and λ are determined self-consistently through the mean-field equations

$$\frac{1}{N} \sum_{\mathbf{k}\sigma} \langle f^\dagger_{\mathbf{k}\sigma} f_{\mathbf{k}\sigma} \rangle + r^2 = 1, \tag{4}$$

$$\frac{1}{N} \sum_{\mathbf{k}\sigma\sigma'} [\mathrm{Re}(V^{\sigma\sigma'}_{\mathbf{k}} \langle c^\dagger_{\mathbf{k}\sigma} f_{\mathbf{k}\sigma'} \rangle) - r\eta\varepsilon_{\mathbf{k}} \delta_{\sigma\sigma'} \langle f^\dagger_{\mathbf{k}\sigma} f_{\mathbf{k}\sigma'} \rangle] + r\lambda = 0. \tag{5}$$

We first illustrate possible phases by setting $t' = 0$. The energy spectra are found as $E_{\mathbf{k}} = -\mu_{\mathbf{k}} \pm \sqrt{m_{\mathbf{k}}^2 + r^2 (v_0 \pm 2\lambda_{\mathrm{so}} \sqrt{\sin^2 \mathbf{k}})^2}$. Clearly, the energy gap is given by $2\sqrt{m_{\mathbf{k}}^2 + r^2 (v_0 - 2\lambda_{\mathrm{so}} \sqrt{\sin^2 \mathbf{k}})^2}$. Hence setting $m_{\mathbf{k}} = 0$ and $v_0 = 2\lambda_{\mathrm{so}} \sqrt{\sin^2 \mathbf{k}}$ determines all gapless phases. More explicitly, gapless phases and corresponding gapless momenta $\mathbf{k}_0$ are determined by $\varepsilon_{\mathbf{k}_0} = (\varepsilon_d + \lambda)/(1 + \eta r^2) \equiv \varepsilon_\lambda, k0$ and $\cos^2 \mathbf{k}_0 \equiv \cos^2 k_{x0} + \cos^2 k_{y0} + \cos^2 k_{z0} = 3 - (v_0/2\lambda_{\mathrm{so}})^2$. It is clear that the effective parameter that tunes the Kondo lattice through different phases is ε_λ. Solutions of $\mathbf{k}_0$ generally form surfaces. As illustrated in Fig. 1(a), there is a large parameter space that supports gapless phases. In addition to gapless regimes, there are phases that have gaps in electronic structures and are characterized by topological indices $(\nu_0; \nu_1, \nu_2, \nu_3)$ [24]. Clearly, going from one gapped phase to another gapped phase with different topological indices, the Kondo lattice has to go through gapless phases. In the special case when $v_0 = 0$, gapless momenta satisfy $\cos^2 \mathbf{k}_0 = 3$ so that $\mathbf{k}_0$ are isolated points at time-reversal invariant momenta: Γ, X, M, and R. These gapless phases are nodal phases with the transition occurring at $\varepsilon_\lambda/t = -6, -2, 2, 6$ as illustrated in Fig. 1(a). Since there are four degenerate zero-energy states at $\mathbf{k}_0$, these phases are Dirac semimetallic phases. In general, t' is nonvanishing and the topological phases are identified in the same way, shown in Fig. 1(b) for $v_0 = 0$. For real materials, $t'/t \sim -0.2$, the strong topological insulator (STI) phase with index (1;000) shrinks, while the (1;111) phase gets enlarged.

Fermionic finite-temperature critical point.—The electronic structures depend on temperature through r and λ. As T increases, r decreases and the coupling between c and d electrons decreases. Eventually c and d decouples at T_K. Here by taking $U \to \infty$ and $v_0 = 0$ in Eq. (2), T_K is estimated as $T_K = 4t \exp[-9\eta t^2/(2\lambda_{\mathrm{so}}^2)]$, where we made use of $D_0 \sim 4t$, $\rho = 1/(6t)$, and $\rho_d |\mu - \epsilon_d| \sim 1$ with $\rho_d = 1/(6\eta t)$ being density of states of d electrons.

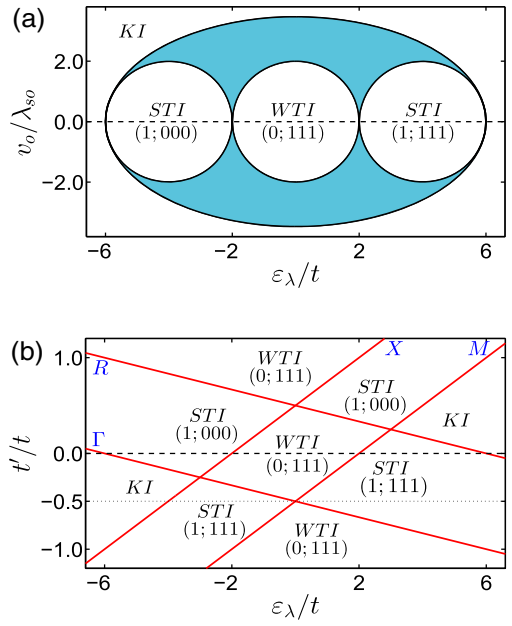

FIG. 1. (a) Topological phase diagram of the Kondo lattice with $t' = 0$. Here $\varepsilon_\lambda \equiv (\varepsilon_d + \lambda/1 + \eta r^2)$ and $(\nu_0;\nu_1,\nu_2,\nu_3)$ are topological indices. Shaded regimes are gapless phases and white regimes are phases with gaps in electronic structures, labeled by a strong topological insulator (STI), a weak topological insulator (WTI), and Kondo insulator (KI) when the valence bands are filled. The gapless phases at $\varepsilon_\lambda/t = -6, -2, 2, 6$ are Dirac semimetallic phases with corresponding Dirac points being at time reversal momenta Γ, X, M, R, respectively. (b) Topological phases for $t' \neq 0$ and $v_0 = 0$. Here solid lines, labeled by Γ, X, M, and R, are phase boundaries with energy gap vanishing at Γ, X, M, and R, respectively.

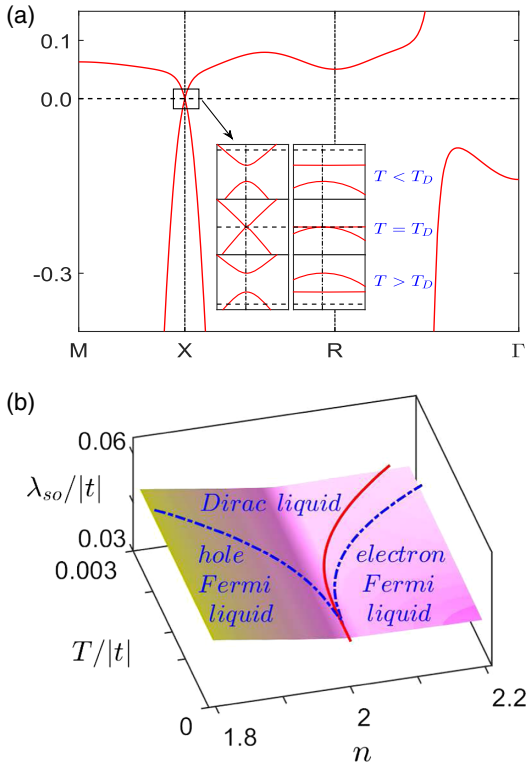

FIG. 2. (a) Emergence of a finite-temperature Dirac point at X point with $n = 2.074$, $t = -1$, $t' = -0.3$, $\lambda_{so} = 0.2$, $\eta = 0.05$, $\varepsilon_d/t = 0.449$. Inset shows relative band positions before hybridization, indicating the occurrence of a band inversion at T_D. (b) Typical surface of T_D^* as a function of n and λ_{so} with $t = -1$, $t' = 0.3$, $\eta = 0.001$, $\varepsilon_d/t = 3.19$. The red line marks critical temperatures T_D at which the chemical potential is at the Dirac point. The blue dashed lines indicate the crossover temperature T^* that separates the Dirac liquid regime from the Fermi liquid regime. As a reference, by using Eq. (2), T_K can be estimated by $4t\exp[-9\eta t^2/(2\lambda_{so}^2)]$, which are in the range $0.026t$–$0.24t$ for $\lambda_{so}/t = 0.03$–0.04 and are at least the order of $10T_D$,

Below T_K, the energy spectrum is found by solving Eqs. (4) and (5). As indicated in Fig. 1(a), when $v_0 = 0$, the system goes through Dirac semimetallic phases in which the energy spectra reduce to $E_{\mathbf{k}}^{\pm} = -\mu_{\mathbf{k}} \pm \sqrt{m_{\mathbf{k}}^2 + 4r^2\lambda_{so}^2 \sin^2 \mathbf{k}}$. By requiring $m_{\mathbf{K}} = 0$ at time reversal momentum $\mathbf{K}$ together with Eqs. (4) and (5), the resulting system possesses Dirac points at some temperatures denoted by T_D^*. Here the chemical potential may not be at the Dirac point. If one further requires that the effective chemical $\mu_{\mathbf{K}}$ vanishes, the system goes through a semimetallic phase with nodal points being at K points. The corresponding temperature is denoted by T_D, which occurs only at properly tuned chemical potential. Figure 2(a) shows that indeed the system goes through a finite-temperature semimetallic phase at $T = T_D$ at three X points by using the proper chemical potential. Clearly, as shown in the inset, the mechanism for the emergent semimetallic phase is the occurrence of a band inversion at X points.

In Fig. 2(b), we show a typical dependence of T_D^* on the electron density n and λ_{so}. T_D^* generally forms a surface so that Dirac points exist in the electronic structures for a large parameter regime. The red line that cuts through different n's shows the temperature T_D. It is clear that finite-temperature Dirac points connect to the zero-temperature QCP smoothly. Hence, the line formed by the temperature T_D extends the QCP and is a critical line that separates the hole Fermi liquid from the electron Fermi liquid.

The effective Hamiltonian near a Dirac point at $\mathbf{K}$ that occurs at T_D^* can be generally expressed as

$$H_{\mathbf{K}} = \begin{pmatrix} \alpha(T - T_D^*)I & \hbar v_F \boldsymbol{\sigma}\cdot\mathbf{q} \\ \hbar v_F \boldsymbol{\sigma}\cdot\mathbf{q} & -\alpha(T - T_D^*)I \end{pmatrix} - \bar{\mu} I, \quad (6)$$

where $\bar{\mu}$ is the effective chemical potential and $\mathbf{q} = \mathbf{k} - \mathbf{K}$ is the deviation of the momentum from $\mathbf{K}$. $H_{\mathbf{K}}$ is valid within a cutoff with $q < q_c$. When the number of electrons is properly tuned so that $\bar{\mu} = 0$, T_D^* reduces to T_D. At T_D, the Kondo lattice is at a finite-temperature critical point. Near T_D, any physical response Q exhibits the scaling behavior as

$$Q(T, T_D, n_i, u) = T^a \Phi\left(\frac{m}{k_B T}, \frac{\bar{\mu}}{k_B T}, \frac{\hbar v_F q_c}{k_B T}, \frac{\hbar^3 v_F^3}{n_{im} u^2 k_B T}\right). \quad (7)$$

Here $m = |\alpha(T - T_D)|$, a is the exponent that characterizes Q, and Φ is the universal scaling function. $n_{im}u^2$ characterizes the disorder strength with n_{im} being the density of impurities and u being the potential strength due to impurities. At $T = T_D$, $m = 0$ and Eq. (7) reduce to the same scaling forms near a zero-temperature QCP. The critical region is thus extended to finite temperatures.

To explore the Fermonic criticality, we examine transport and thermodynamical measurements. For this purpose, it is necessary to include temperature effects due to the quasiparticle lifetime τ. Following Ref. [25], we obtain the inverse quasiparticle lifetime as $1/\tau = (rV_K/\epsilon_d + \lambda - \mu)^2[(\hbar\omega)^2 + \pi^2(k_B T)^2/2(\epsilon_d + \lambda - \mu)]$ with $\hbar\omega$ being the energy of the quasiparticle [16]. By including the self-energy of holons in the free energy, one obtains the heat capacity [16]. The contribution to $C(T)$ due to Dirac points obeys the scaling law with exponent $a = 3$ [16]. However, due to the fermionic nature, the contribution to $C(T)$ mainly comes from states near the Fermi energy. Hence, unlike the classical critical point, $C(T)$ is smooth crossing $T = T_D$ as indicated in Fig. 3(a). On the other hand, the electric transport is determined by available states near the Fermi energy and is expected to be suppressed. By using the Kubo formula, the resistivity $\rho(T)$ is computed in the self-consistent Born approximation [26]. The critical exponent is found to be $a = -1$ [16]. Figure 3(b) shows how $\rho(T)$ changes as the system goes through the Dirac semimetallic phase. A peak is exhibited due to the decreasing density of states. However, due to finite temperature excitations, ρ is not infinite at T_D. Similarly, the magnetic susceptibility $\chi(T)$ also exhibits the Dirac semimetallic phase. The energy of a Landau level in a magnetic field $B\hat{z}$ is given by $\epsilon^{ss'}_{n,q_z} = -\bar{\mu} + s\sqrt{(E_{q_z} + s'\mu_B B)^2 + n\hbar^2\omega_B^2}$ with $s, s' = \pm 1$, q_z being the wave vector along the z axis, μ_B being the Bohr magneton,

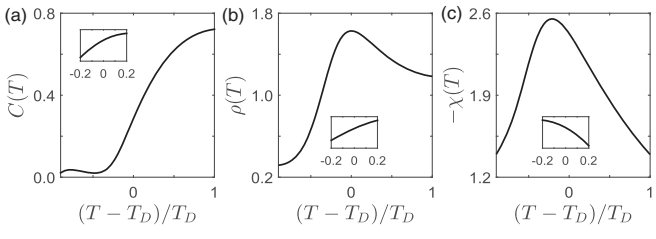

FIG. 3. Temperature dependence of (a) heat capacity in units of k_B, (b) resistivity in units of $0.1\pi^2\hbar^3 v_F/n_D e^2\epsilon_c$, (c) magnetic susceptibility in units of $n_D e^2 v_F/3\pi^2 c^2\hbar$. Inset figures show the corresponding scaling functions. Here $C(T)$, $\rho(T)$, and $\chi(T)$ exhibit scaling laws near T_D with exponents a being 3, -1, and 0, respectively.

$E_{q_z} = \sqrt{m^2 + \hbar^2 v_F^2 q_z^2}$, and $\hbar\omega_B = \sqrt{2eBv_F^2/c\hbar}$. $\chi(T)$ is then found by computing the grand potential Ω and $\chi(T) = -(\partial^2\Omega/\partial B^2)|_{B\to 0}$ [16]. Figure 3(c) shows the computed $\chi(T)$ with the scaling exponent being $a = 0$. The diamagnetic response is enhanced due to the $n = 0$ Landau level that resides at the Fermi energy [26]. For 3D Dirac semimetals, the enhancement gets broadened as the $n = 0$ Landau level becomes a 1D band along the field direction [16].

Finally, we analyze effects on critical scalings due to the off-site Coulomb interaction $H_C = (e^2/2\epsilon)\sum_{i,j}[n(\mathbf{r}_i)n(\mathbf{r}_j)/|\mathbf{r}_i - \mathbf{r}_j|]$, where $n(\mathbf{r}_i)$ is the electron density at i site. On the T_D^* surface, the effective Hamiltonian is $H_{\mathbf{K}} + H_C$. As shown in Ref. [12] for graphene, there is a regime dictated by the Dirac point, known as a Dirac liquid, in which the Coulomb interaction induces logarithmic corrections in response functions. The dimensionless parameter for the correction is $\bar{\lambda} = e^2/(\epsilon v_F\hbar)$. Following Ref. [12], a RG analysis is performed by integrating out modes in $q_c/b < q < q_c$ with $\lambda(\bar{b})$ and the temperature $T(b)$ on the T_D^* surface obeying $[d\bar{\lambda}(b)/d\ln(b)] = -\bar{c}\,\bar{\lambda}(b)^2$ $[dT(b)/d\ln b] = T(b)[1 - \bar{c}\,\bar{\lambda}(b)]$, where $\bar{c} = 2/3\pi$. Hence H_C is marginal and its effects lie in the regime bounded by the crossover scale b^*. Setting $n(b^*) = n_0$ and $T(b^*) = T_0 = \hbar v_F q_c$ with n_0 and T_0 being the electron density and temperature scale in the high temperature region [12], the crossover temperature is found to be $T^*(n) = T_0|n - 2|^{1/3}[1 + \bar{c}(\bar{\lambda}/3)\ln(n_0/|n - 2|)]$. Here T_0 weakly depends on T_D^* and hence T^* is roughly a border line. In Fig. 2(b), T^* is indicated by blue dashed lines. Inside T^* in the Dirac liquid regime, responses of electrons get corrections by factors of $\Delta(T) = [1 + \bar{c}\,\bar{\lambda}\ln(T_0/T)]$. Replacing v_F by $\Delta(T)v_F$, we find that the diamagnetic susceptibility χ gets a further enhancement by the factor $\Delta(T)$ in the Dirac liquid regime, while the conductivity and the heat capacity get suppressed by factors of $\Delta(T)$ and $\Delta^3(T)$, respectively.

Discussion and conclusion.—The fermionic finite-temperature critical point also occurs at 2D [16]. Experimentally, the critical point can be more easily realized in 2D Kondo lattices, which are formed by introducing adatoms on two-dimensional materials such as graphene [27]. These critical points are protected as they result from transitions between two topological phases and transitions must go through gapless phases. Therefore, one expects that Dirac semimetallic phases survive even if fluctuations that are beyond the mean-field theory are included. In real materials, λ_{so} and n are fixed so that the system is generally not at QCP. However, our results show that quite generally, by increasing temperature and tuning the electron number, the Kondo lattice will pass through T_D. Hence we expect the results on measurements shown in Fig. 3 are applicable to materials such as SmB_6. In particular, a broad peak in resistivity measurement similar to Fig. 3(b) was observed in

experiments [28], indicating that the Dirac semimetallic phase may have been already observed.

In conclusion, we demonstrate that instead of always being a gapped topological insulator below the Kondo temperature shown in Ref. [14], the Kondo lattice can become gapless by going through a finite-temperature topological transition from a STI phase to a WTI phase. At the transition, the Kondo lattice is a Dirac semimetal, which exhibits finite-temperature relativistic symmetry with nontrivial thermal responses. Our work opens a new pathway to access the Dirac semimetallic phase and explore the fermionic critical point in the same system.

This work was supported by Ministry of Science and Technology (MoST), Taiwan. We also acknowledge support from TCECM and Academia Sinica Research Program on Nanoscience and Nanotechnology, Taiwan.

[1] K. S. Novoselov *et al.*, Science **306**, 666 (2004).
[2] A. H. Castro Neto, F. A. H. Guinea, N. M. R. Peres, K. S. Novoselov, and A. K. Geim, Rev. Mod. Phys. **81**, 109 (2009).
[3] M. A. Hasan and C. L. Kane, Rev. Mod. Phys. **82**, 3045 (2010).
[4] X. L. Qi and S.-C. Zhang, Rev. Mod. Phys. **83**, 1057 (2011).
[5] S. Cahangirov, M. Topsakal, Akturk, H. Sahin, and S. Ciraci, Phys. Rev. Lett. **102**, 236804 (2009).
[6] Z. K. Liu *et al.*, Science **343**, 864 (2014).
[7] S. Borisenko, Q. Gibson, D. Evtushinsky, V. Zabolotnyy, B. Buchner, and R. J. Cava, Phys. Rev. Lett. **113**, 027603 (2014).
[8] M. Neupane *et al.*, Nat. Commun. **5**, 3786 (2014).
[9] T. O. Wehling, A. M. Black-Schaffer, and A. V. Balatsky, Adv. Phys. **63**, 1 (2014).
[10] S. Q. Shen, W. Y. Shan, and L. Z. Lu, SPIN **01**, 33 (2011).
[11] T. Sato, S. Segawa, K. Kosaka, S. Souma, K. Nakayama, K. Eto, T. Minami, Y. Ando, and T. Takahashi, Nat. Phys. **7**, 840 (2011).
[12] D. E. Sheehy and J. Schmalian, Phys. Rev. Lett. **99**, 226803 (2007).
[13] S. M. Young, S. Zaheer, J. C. Y. Teo, C. L. Kane, E. J. Mele, and A. M. Rappe, Phys. Rev. Lett. **108**, 140405 (2012).
[14] M. Dzero, K. Sun, V. Galitski, and P. Coleman, Phys. Rev. Lett. **104**, 106408 (2010).
[15] J. R. Schrieffer and P. A. Wolff, Phys. Rev. **149**, 491 (1966).
[16] See Supplemental Material at http://link.aps.org/supplemental/10.1103/PhysRevLett.116.177002 for the derivation of the effective Kondo model and renormalization group equations, and for details of the computation on physical response functions, which includes Refs. [15,17,20,17–21]
[17] P. W. Anderson, J. Phys. C **3**, 2436 (1970).
[18] K. G. Wilson, Rev. Mod. Phys. **47**, 773 (1975).
[19] H. R. Krishna-murthy, J. W. Wilkins, and K. G. Wilson, Phys. Rev. B **21**, 1003 (1980).
[20] R. Bulla, T. A. Costi, and T. Pruschke, Rev. Mod. Phys. **80**, 395 (2008).
[21] N. Read and D. M. Newns, J. Phys. C **16**, 3273 (1983).
[22] C. Lacroix and M. Cyrot, Phys. Rev. B **20**, 1969 (1979).
[23] M. Zarea, S. E. Ulloa, and N. Sandler, Phys. Rev. Lett. **108**, 046601 (2012).
[24] L. Fu, C. L. Kane, and E. J. Mele, Phys. Rev. Lett. **98**, 106803 (2007).
[25] A. J. Millis and P. A. Lee, Phys. Rev. **35B**, 3394 (1987);
A. Auerbach and K. Levin, Phys. Rev. Lett. **57**, 877 (1986).
[26] N. H. Shon and T. Ando, J. Phys. Soc. Jpn. **67**, 2421 (1998).
[27] T. O. Wehling, A. V. Balatsky, M. L. Katsnelson, A. I. Lichtenstein, and A. Rosch, Phys. Rev. B **81**, 115427 (2010).
[28] A broad peak in resistivity is observed near 10 K in SmB_6, see D. J. Kim, J. Xia, and Z. Fisk, Nat. Mater. **13**, 466 (2014).